

Modelling of Flow Dynamics of an Incompressible Viscous Fluid in a Channel with Solid Obstruction of Variable Length

Deepak Kumar¹ and R.K Malik²

¹Assistant Professor, Department of Mechanical and Automation Engineering, Amity University Gurgaon, India

²Professor of Hydrology and Water Resources Engineering, Department of Civil Engineering, Amity University Gurgaon, India

E-mail: deepak209476@gmail.com

Contact No: +91-9416627599

Abstract— In this study, the time-independent laminar flow of a viscous, incompressible fluid in two-dimensions was analyzed using Navier–Stokes equations with continuity equation as an incompressibility constraint and vorticity–stream function approach. The fluid was allowed to flow in a rectangular channel obstructed by a solid rectangular plate of variable length with uniform incident velocity. The CFD computer code Flex PDE was used to analyze the flow dynamics. It was observed that by increasing the blockage ratio, the maximum values of the stream function as well as the maximum value of the velocity decreased at the obstruction and the size of vortex increased. It was also observed that with the increase in blockage ratio the region of low pressure increased behind the obstruction.

Keywords— Channel flow, Rectangular obstruction, Two-dimensional flow dynamics, Navier-Stokes equations, Vorticity-Stream function, Flex PDE, Reynolds number.

INTRODUCTION

In the pipes and channels, many a times it has been observed that the fluid flow is constricted by obstructions of different shapes and sizes affecting the fluid flow dynamics. The understanding of the complexities of the fluid flows arising out of these constrictions is of importance in computational fluid dynamics. Researchers in this field have introduced different types of mathematical methods and techniques to understand the complexities of the fluid flows under different kinds of obstructions.

Roshko [1] investigated the effects of vortex formations and bluff body similarity using dimensional analysis of a wake model. He gave an empirical relation between the universal Strouhal number and the wake Reynolds number (R_w). Using this relation, drag was calculated from the shedding frequency measurements. In his work, different bluff bodies were correlated in a single relation. Greenspan [2] analyzed the numerical study of steady, viscous, incompressible flow in a channel with a step in two dimensions. He showed the variation of streamlines and equi-vorticity at different Reynolds numbers and concluded that as the Reynolds number is increased, the size of the right vortex also increases. Zdravkovich [3] presented a review of flow interference between the two circular cylinders in various arrangements for different separation distances and Reynolds numbers. In side-by-side arrangement to the approaching flow of two circular cylinders interference in drag coefficient was observed for a separation distance smaller than five cylinder diameters. The flow pattern in side-by-side arrangements showed a bi-stable nature. He further observed that for a separation distance greater than two, the process of the vortex formation of both cylinders was exactly the same as that of the single cylinder and when the separation distance becomes smaller, the bulk flow between the two cylinders deflected to one side or the other can equally take place. Valencia [4] performed the experimental investigations on the wake interference of a row of normal flat plates consisting of two, three and four plates arranged side-by-side in a uniform flow with Reynolds numbers of about 10^4 . Braza et al. [5] used a second-order finite volume method and analyzed the dynamic characteristics of the pressure and velocity fields of the unsteady, incompressible and laminar wake behind a circular cylinder. Different vortex and physical aspects of the initiation of vortex shedding as well as the interactions of the velocity and the pressure in the wake, outside the wake and near wake were analyzed in their work.

Gera et al. [6] carried out a numerical simulation for a two-dimensional unsteady laminar flow past a square cylinder for the Reynolds numbers in the range of 50-250 and captured the features of flows past a square cylinder in a domain with the use of CFD code. The variation of Strouhal number with Reynolds number was found from this analysis and it was found that upto Reynolds number 50, the flow was observed to be steady and between the Reynolds numbers 50 to 55, instability occurred and vortex shedding appeared and flow became unsteady. Kumaret al.[7] studied the flow past a rotating circular cylinder experimentally in a water tunnel at Reynolds numbers of 200, 300, and 400 and non-dimensional rotation rates α (ratio of surface speed of the cylinder to the free stream velocity) varying from 0 to 5. They presented global view of the wake structure at the three Reynolds numbers and various rotation rates. It was found that for $0 < \alpha < 1.95$, regular periodic vortex shedding was observed with vortex shedding suppression occurring at $\alpha = 1.95$ for all the Reynolds numbers. The Reynolds number was observed to influence the wake morphology more strongly near the vortex shedding suppression rotation rate. Lam and Leung [8] investigated the vortices behind a long flat plate inclined at a small angle of attack to a main flow stream. In this study, velocity fields were obtained at three angles of attack 20° , 25° and 30° and at a Reynolds number $Re \approx 5,300$. Vikram et al. [9] analyzed the numerical investigation of two-dimensional unsteady flow past two square cylinders with in-line arrangements in a free stream to investigate the influences on the size of the eddy, velocity, frequency of vortex shedding, pressure coefficient and lift coefficient by varying pitch to perimeter ratio of two square cylinders. It was found that the size of the eddy and the monitored velocity in between the square cylinders increased with the increase in the pitch to perimeter ratio. In this investigation, frequency of vortex shedding was found to be same in between the cylinders and in the downstream of the cylinder and the pressure distribution near to the surface of the cylinder was observed to be quite low due to the viscous effects. In this analysis, the upstream cylinder was found to experience higher lift compared to the downstream cylinder.

Domaet al. [10] described the motion of the steady flow of a viscous incompressible fluid passing a rectangular plate and simulated numerically. In this study, the Reynolds number was varied as 0.5, 1, 10, 20, 100, 200 and 300 and the variation of streamlines was studied along with the pressure force, velocity magnitude, vorticity magnitude. Gowda and Tulapurkaraz [11] studied the flow through and around a parallel-walled channel with an obstruction (flat plate) placed at the channel inlet. Depending on the position of the obstruction, the flow inside the channel was observed to be in a direction opposite to that of outside, stagnant or in the same direction as outside but with reduced magnitude. The parameters that varied were the gap between the obstruction and the entry to the channel, the length of the channel and the Reynolds number. In this study, the maximum value of the reverse flow velocity was found to be about 20 % of that of the flow outside and the maximum forward velocity inside the channel (when it occurred) was observed to be only about 65% of the outside velocity even for very large gaps between the obstruction and the channel entrance. Bhattacharyya and Maiti [12] gave information about the uniform flow past a long cylinder of square cross-section placed parallel to a plane wall. In this study, the maximum gap between the plane walls to the cylinder was taken to be 0.25 times the cylinder height and found that the critical value of the gap height for which vortex shedding was suppressed depended on the Reynolds number which was based on the height of the cylinder and the incident stream at the surface of the cylinder. Kabir et al. [13] studied the numerical simulation of the reverse flow phenomena in a channel with obstruction geometry of triangular, circular, semi-circular and flat plate at the entry. In this study, the simulations were performed for different gap to width ratios and for different Reynolds numbers. The simulation results predicted the occurrence of reverse flow and existence of other flow features such as vortex shedding.

In this study, the influence of the different ratios of the length of the rectangular solid obstruction to the channel width termed as the blockage ratio on the velocity and pressure fields and the stream patterns was investigated numerically using the Navier-Stokes equations along with the continuity equation as a compressibility constraint and the stream and vorticity mathematical formulations for the two-dimensional, steady, laminar flow of incompressible and viscous fluid in a rectangular channel.

GOVERNING MATHEMATICAL FORMULATION

The flow dynamics for incompressible (divergence-free) Newtonian fluid within the flow domain is described by the Navier-Stokes equations (momentum equations- a set of second-order partial differential equations relating first and second derivatives of fluid velocity) under isothermal and steady state conditions neglecting gravity force in the Laplace formulation along with the continuity equation for the conservation of mass as:

$$(\mathbf{U} \cdot \nabla) \mathbf{U} + (\nabla p)/\rho - \nu \nabla^2 \mathbf{U} = 0 \quad (1)$$

$$\nabla \cdot \mathbf{U} = 0 \quad (2)$$

Where the first term in Eq.(1) is the inertia force due to the time-independent convective acceleration associated with the change in velocity vector $\mathbf{U}(x, y)$ over position causing non-linearity. ∇p is the gradient of pressure force $p(x, y)$, ρ is the density of the fluid i.e. water in this analysis, ν is the kinematic viscosity (ratio of the dynamic viscosity μ and the density ρ) of the fluid under consideration. The divergence of velocity vector $\nabla \cdot \mathbf{U}$ representing the continuity equation acts as the incompressibility constraint for the Navier-Stokes equations ensuring the conservation of mass of the fluid under consideration.

In this study for the two-dimensional flow under above stated assumptions, the Navier-Stokes equations (Eq.1) and the continuity equation (Eq. 2) in the primitive variable formulation in Cartesian coordinate system are written as:

$$\left(u \frac{\partial u}{\partial x} + v \frac{\partial u}{\partial y}\right) = \frac{1}{\rho} \left[-\frac{\partial p}{\partial x}\right] + \nu \left(\frac{\partial^2 u}{\partial x^2} + \frac{\partial^2 u}{\partial y^2}\right) \quad (3)$$

$$\left(u \frac{\partial v}{\partial x} + v \frac{\partial v}{\partial y}\right) = \frac{1}{\rho} \left[-\frac{\partial p}{\partial y}\right] + \nu \left(\frac{\partial^2 v}{\partial x^2} + \frac{\partial^2 v}{\partial y^2}\right) \quad (4)$$

$$\frac{\partial u}{\partial x} + \frac{\partial v}{\partial y} = 0 \quad (5)$$

Where u and v are the components of the velocity vector \mathbf{U} in the directions x (along the channel) and y (across the channel), respectively. Eq.(1) was converted to non-dimensional form by scaling the terms using characteristic (reference) length (L) and characteristic (reference) velocity (U^*). In this analysis, the characteristic length and the characteristic velocity were taken as the channel width and the mean velocity of the flow, respectively. The dimensionless form of Navier-Stokes equations for the two-dimensional flow in the vector form is written as:

$$(\bar{\mathbf{U}} \cdot \bar{\nabla}) \bar{\mathbf{U}} + \bar{\nabla} \bar{p} - \frac{1}{Re} (\bar{\nabla}^2 \bar{\mathbf{U}}) = 0 \quad (6)$$

Where Re is the Reynolds Number (ratio of inertial to viscous forces) and the dimensionless variables are as under:

$$\bar{x} = \frac{x}{L} \quad ; \quad \bar{y} = \frac{y}{L} \quad ; \quad \bar{\mathbf{U}} = \frac{\mathbf{U}}{U^*} \quad ; \quad \bar{p} = \frac{p}{P}$$

$$\frac{\partial}{\partial \bar{x}} = \bar{\nabla} = L \frac{\partial}{\partial x} \quad ; \quad \frac{\partial}{\partial \bar{y}} = \bar{\nabla} = L \frac{\partial}{\partial y}$$

$$\frac{\partial^2}{\partial \bar{x}^2} = \bar{\nabla}^2 = L^2 \frac{\partial^2}{\partial x^2} \quad ; \quad \frac{\partial^2}{\partial \bar{y}^2} = \bar{\nabla}^2 = L^2 \frac{\partial^2}{\partial y^2}$$

Here, the two dimensionless groups in the non-dimensional Navier-Stokes equations are as:

$$\frac{P}{\rho U^{*2}} \text{ and } \frac{\mu}{\rho U^* L}$$

The inverse of the dimensionless group $\left(\frac{\mu}{\rho U^* L}\right)$ is the Reynolds number. For two-dimensional fluid flow, Eqs. (3 and 4) in the non-dimensional form are written as:

$$\bar{u} \frac{\partial \bar{u}}{\partial \bar{x}} + \bar{v} \frac{\partial \bar{u}}{\partial \bar{y}} = -\frac{\partial \bar{p}}{\partial \bar{x}} + \frac{1}{Re} \left(\frac{\partial^2 \bar{u}}{\partial \bar{x}^2} + \frac{\partial^2 \bar{u}}{\partial \bar{y}^2}\right) \quad (7)$$

$$\bar{u} \frac{\partial \bar{v}}{\partial \bar{x}} + \bar{v} \frac{\partial \bar{v}}{\partial \bar{y}} = -\frac{\partial \bar{p}}{\partial \bar{y}} + \frac{1}{Re} \left(\frac{\partial^2 \bar{v}}{\partial \bar{x}^2} + \frac{\partial^2 \bar{v}}{\partial \bar{y}^2}\right) \quad (8)$$

Where $\bar{u} = \frac{u}{U^*} \quad ; \quad \bar{v} = \frac{v}{U^*}$

The continuity equation (Eq.5) in the non-dimensional form is written as:

$$\frac{U^*}{L} \left[\frac{\partial \bar{u}}{\partial \bar{x}} + \frac{\partial \bar{v}}{\partial \bar{y}} = 0 \right] \text{ or } \frac{\partial \bar{u}}{\partial \bar{x}} + \frac{\partial \bar{v}}{\partial \bar{y}} = 0 \quad (9)$$

The vorticity-stream function formulation was employed in which the derived variables in terms of the vorticity vector ω (curl of the flow velocity vector) is written as:

$$\omega = \nabla \times U \quad (10)$$

The stream vorticity vector for two-dimensional case is written as:

$$\omega = \frac{\partial v}{\partial x} - \frac{\partial u}{\partial y} \quad (11)$$

For developing the streamlines (lines with constant value of stream function) pattern, the stream function was used. The usefulness of the stream function $\psi(x, y)$ lies in the fact that the velocity components in the x and y direction at a given point are given by the partial derivatives of the stream function at that point and also the two-dimensional continuity equation (Eq.5) implies the existence of a function called the stream function $\psi(x, y)$ such that

$$\frac{\partial \psi}{\partial x} = -v \text{ and } \frac{\partial \psi}{\partial y} = u \quad (12)$$

By combining the above definitions with Eqs.(7 and 8), the non-pressure vorticity transport equation for steady state condition is obtained as:

$$u \frac{\partial \omega}{\partial x} + v \frac{\partial \omega}{\partial y} = \frac{1}{Re} \left(\frac{\partial^2 \omega}{\partial x^2} + \frac{\partial^2 \omega}{\partial y^2} \right) \quad (13)$$

The incompressibility constraint is satisfied by expressing the velocity vector in terms of stream function as given in Eq. (12). By coupling the Eq. (12) and the scalar vorticity ($\omega = \nabla \times U$, k ; k being the unit vector in z direction) of Eq. (11), the two-dimensional mathematical formulation for the stream function $\psi(x, y)$ in the elliptic form (Poisson equation) is obtained as:

$$\frac{\partial^2 \psi}{\partial x^2} + \frac{\partial^2 \psi}{\partial y^2} = -\omega \text{ or } \nabla^2 \psi = -\omega \quad (14)$$

The stream function $\psi(x, y)$ was found from the vorticity function (Eq. 14).

PROBLEM DESCRIPTION

In this study, the two-dimensional steady and laminar flow of an incompressible and viscous fluid under isothermal condition normal to a solid flat rectangular obstruction (plate) of a finite length in a fluid flowing in a pipe of rectangular cross-section (referred as channel) as shown in Fig. A was considered for analyzing the influence of the ratio of the length of the solid rectangular obstruction to the channel width termed as blockage ratio h on the nature of flow dynamics. The numerical simulations were carried out for $h = 0.3, 0.5, 0.7$ and 0.9 for the Reynolds number (Re) equal to 100. In the present investigation the problem has been computed by applying boundary conditions as follows.

- (a) At inlet – Uniform flow ($U = 1.0, V = 0$)
- (b) At outlet boundary – Atmospheric pressure ($P = 0$)
- (c) On the surface – No slip condition ($U = V = 0.0$)

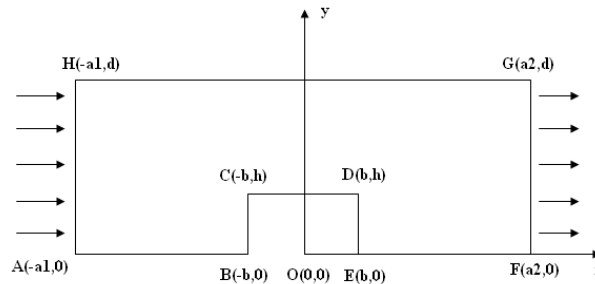


Fig. A

NUMERICAL SIMULATION

For simulating the stream line patterns, velocity and pressure distributions in the flow regime under study were simulated using CFD computer code Flex PDE (A flexible solution system for partial differential equations by PDE solutions Inc., www.pdesolutions.com). This code utilizes the finite element numerical solver performing the operations necessary to turn a description of a partial differential equations system into a finite element model, solve the system, and present graphical and tabular output of the results. It performs the entire range of functions necessary to solve partial differential equation systems: an editor for preparing scripts, a mesh generator for building finite element meshes, a finite element solver to find solutions, and a graphics system to plot the results.

Flex PDE solves systems of first or second order partial differential equations in one, two or three-dimensional Cartesian geometry, in one-dimensional spherical or cylindrical geometry, or in axi-symmetric two-dimensional geometry. The system may be steady-state or time-dependent. The equations can be linear or nonlinear. (Flex PDE automatically applies a modified Newton-Raphson iteration process in nonlinear systems.) Flex PDE is a fully integrated PDE solver, combining several internal facilities to provide a complete problem solving system with the following facilities.

- A symbolic equation analyzer expands defined parameters and equations, performs spatial differentiation, and symbolically applies integration by parts to reduce second order terms to create symbolic Galerkin equations. It then symbolically differentiates these equations to form the Jacobian coupling matrix.
- A mesh generation facility constructs a triangular or tetrahedral finite element mesh over a two or three-dimensional problem domain. In two- dimensions, an arbitrary domain is filled with an unstructured triangular mesh. In three-dimensional problems, an arbitrary two-dimensional domain is extruded into third dimension and cut by arbitrary dividing surfaces. The resulting three-dimensional Fig. is filled with an unstructured tetrahedral mesh.
- A Finite Element numerical method facility selects an appropriate solution scheme for steady-state, time-dependent or eigen value problems with separate procedures for linear and nonlinear systems. The finite element basis may be linear, quadratic or cubic.
- An adaptive mesh refinement procedure measures the adequacy of the mesh and refines the mesh wherever the error is large. The system iterates the mesh refinement and solution until a user-defined error tolerance is achieved.
- A dynamic time step control procedure measures the curvature of the solution in time and adapts the time integration step to maintain accuracy.

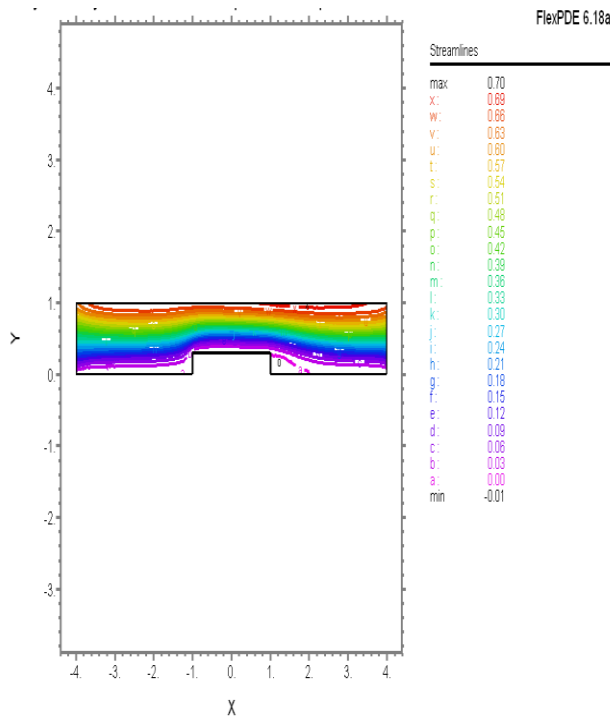
RESULTS AND DISCUSSION

The streamline patterns are shown in Figs. 1, 5, 9 and 13 at blockage ratios of 0.3, 0.5, 0.7 and 0.9, respectively. It was observed that as we go away from the obstruction in the y-direction the values of stream function increased at different blockage ratios. Also the maximum values of stream function were observed to be 0.70, 0.45, 0.17 and 0.16 at blockage ratios of 0.3, 0.5, 0.7 and 0.9, respectively. It is seen from these simulated values of stream function that as the blockage ratio was increased the maximum value of the stream function decreases. Further from these Figs. it was also observed that the size of vortex formed in the right of the obstruction got enlarged as the blockage ratio increased from 0.3 through 0.9.

The velocity distribution for different blockage ratios were shown in Figs. 2, 6, 10, and 14 and from these Figs. the maximum values of the velocity in x-direction were observed to be 1.47, 1.31, 0.79 and 0.78 at the obstruction for these blockage ratios, respectively.

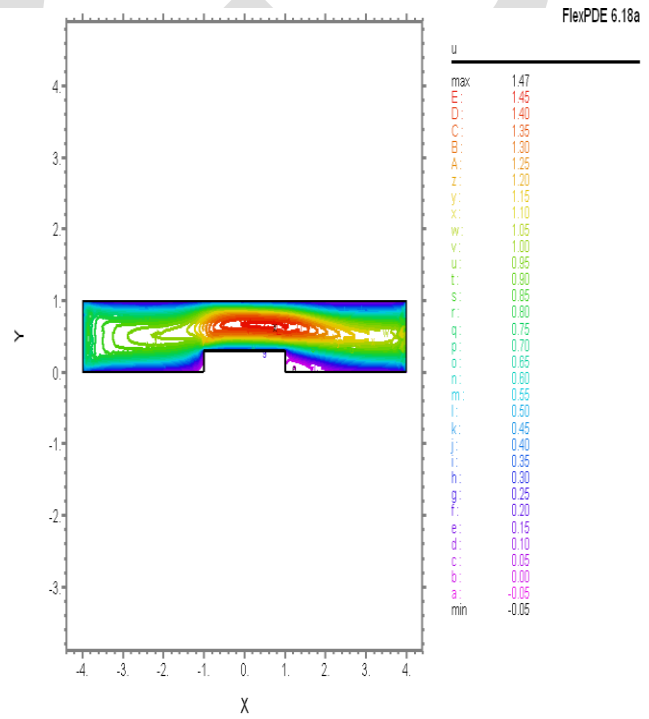
Further it was observed that the velocity decreased past the obstruction. These simulated values of maximum velocities revealed that as the blockage ratio increases from 0.3 to 0.7 the variation in the magnitude of the maximum velocities were higher in comparison to those when the blockage ratio increased from 0.7 to 0.9.

The flow patterns were shown in Figs. 3,7,11 and 15. It was seen from these Figs. that the flow reversed its direction in the right corner of the obstruction. It is seen from these Figs. that the area of the reversed flow region increased with the increase in blockage ratio. This is because the pressure behind the obstruction is low in comparison to the pressure in other region of the flow. It was also observed that as the blockage ratio was increased the magnitude of the flow decreased. The pressure profiles were shown in Fig. 4,8,12 and 16 for different blockage ratios. It is seen from these Figs. that as the blockage ratio increases the pressure at the obstruction decreases while the region of low pressure increased behind the obstruction.



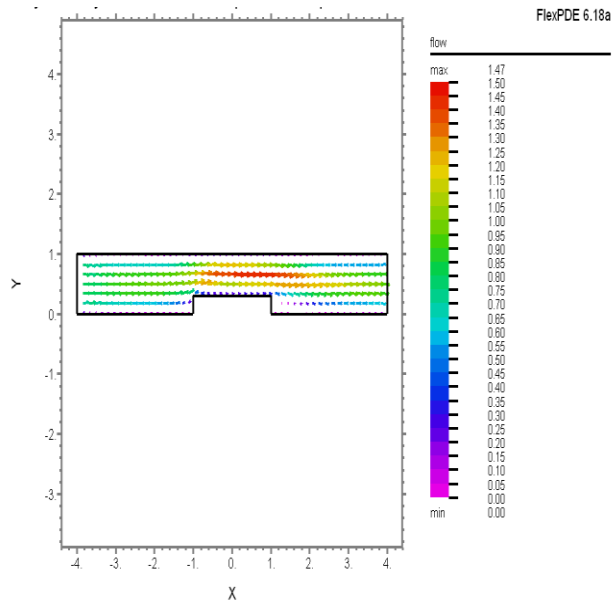
lowvisc: Grid#2 P2 Nodes=814 Cells=363 RMS Err= 2.6492
 Integral= 2.423202

Fig. 1: Streamlines at $h = 0.3$



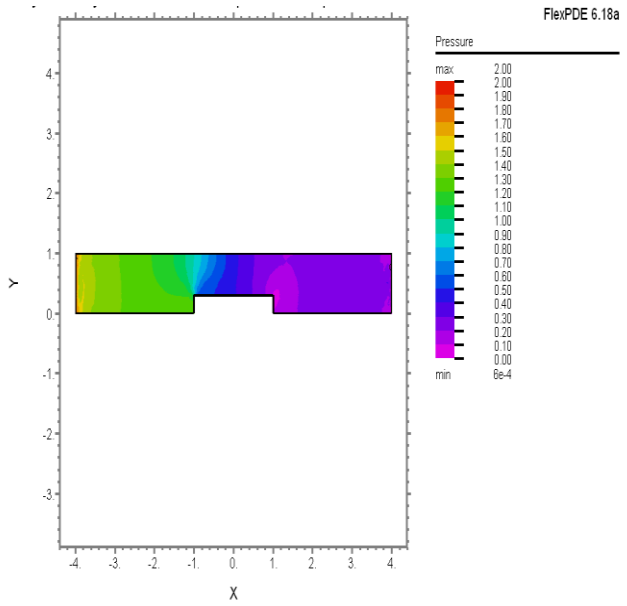
lowvisc: Grid#2 P2 Nodes=814 Cells=363 RMS Err= 2.6492
 Integral= 5.468413

Fig.2: Velocity in x – direction at $h=0.3$



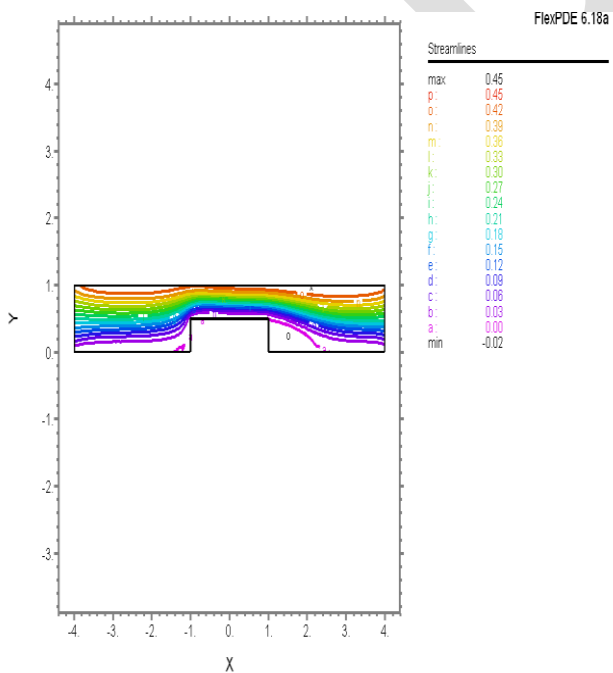
lowvisc: Grid#2 P2 Nodes=814 Cells=363 RMS Err= 2.6492

Fig. 3: Flow at h = 0.3



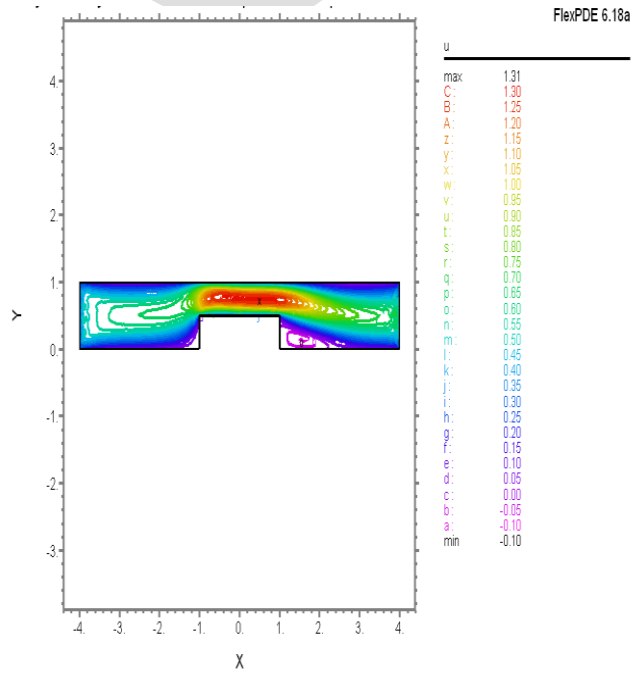
lowvisc: Grid#2 P2 Nodes=814 Cells=363 RMS Err= 2.6492
 Integral= 5.124343

Fig.4: Pressure at h = 0.3



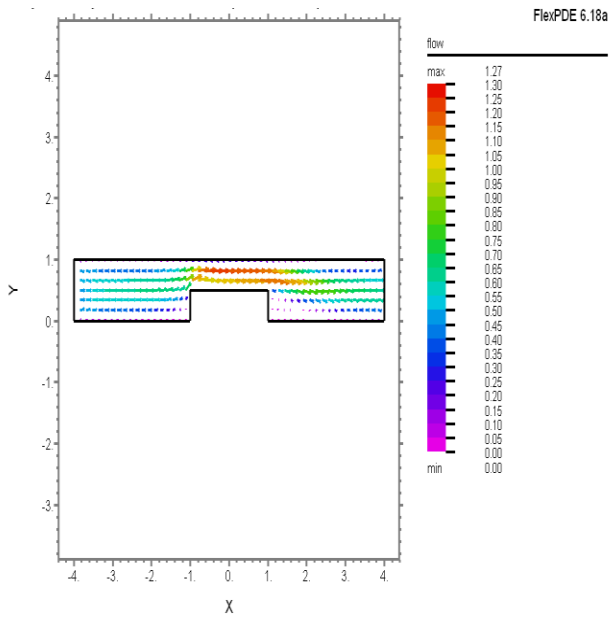
lowvisc: Grid#2 P2 Nodes=819 Cells=364 RMS Err= 1.291
 Integral= 1.391370

Fig.5: Streamlines at h = 0.5



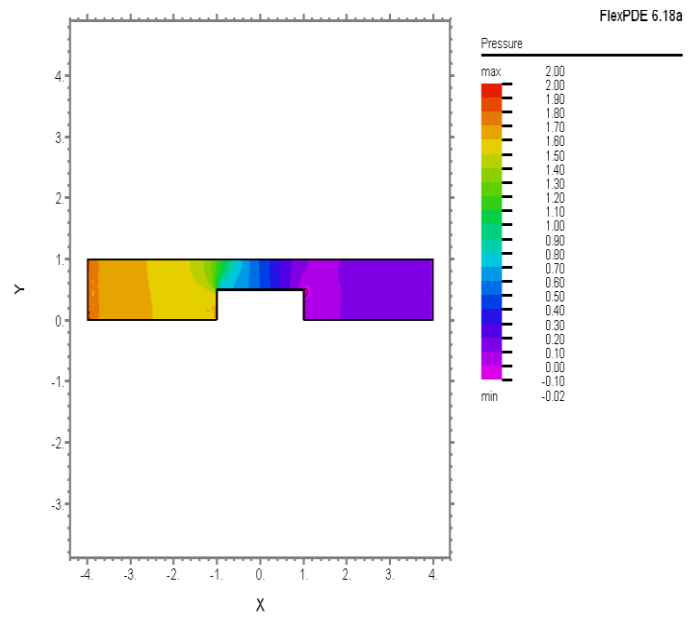
lowvisc: Grid#2 P2 Nodes=819 Cells=364 RMS Err= 1.291
 Integral= 3.495525

Fig.6: Velocity in x – direction at h =0.5



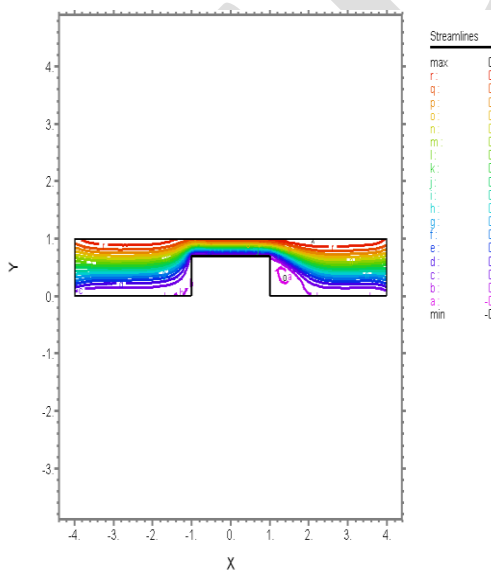
lowvisc: Grid#2 P2 Nodes=819 Cells=364 RMS Err= 1.291

Fig.7: Flow at h = 0.5



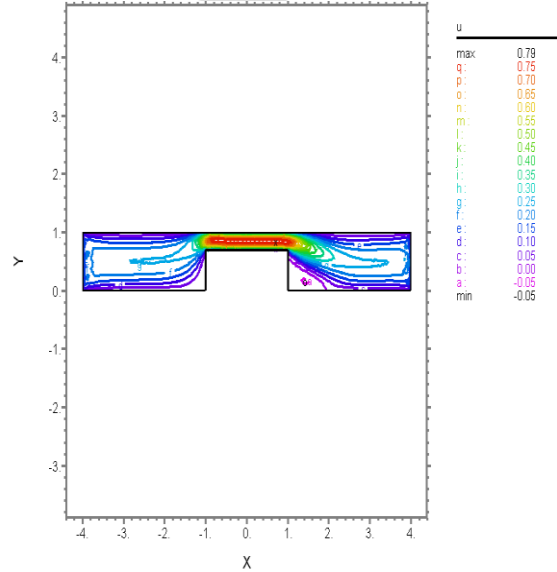
lowvisc: Grid#2 P2 Nodes=819 Cells=364 RMS Err= 1.291
 Integral= 5.692239

Fig.8: Pressure at h = 0.5



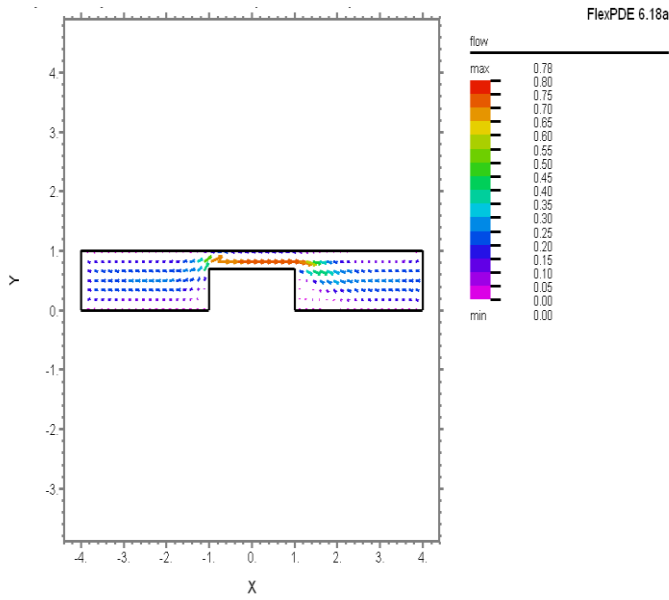
lowvisc: Grid#2 P2 Nodes=814 Cells=357 RMS Err= 1.0487
 Integral= 0.482650

Fig.9: Streamlines at h = 0.7



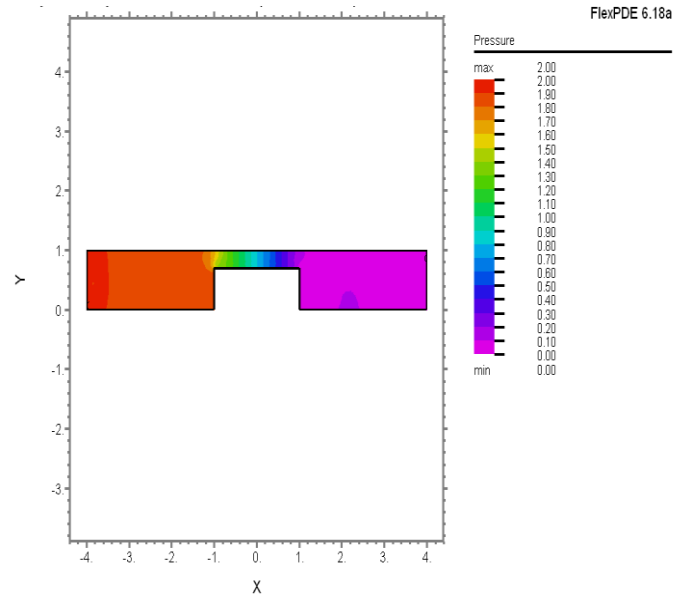
lowvisc: Grid#2 P2 Nodes=814 Cells=357 RMS Err= 1.0487
 Integral= 1.292387

Fig.10: Velocity in x – direction at h = 0.7



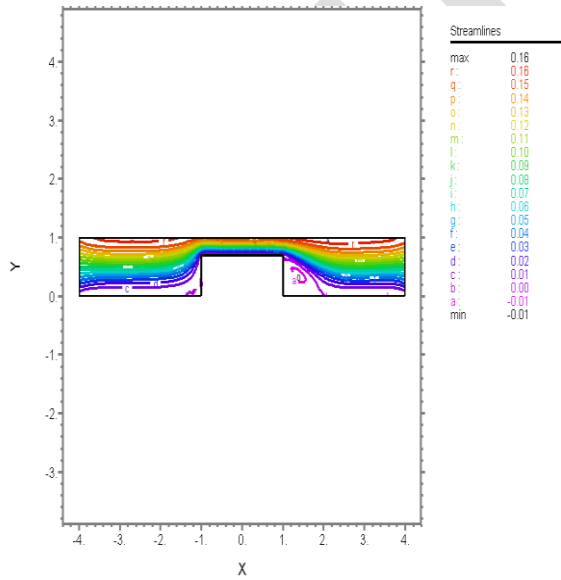
lowvisc: Grid#2 P2 Nodes=814 Cells=357 RMS Err= 1.0487

Fig.11:Flow at $h = 0.7$



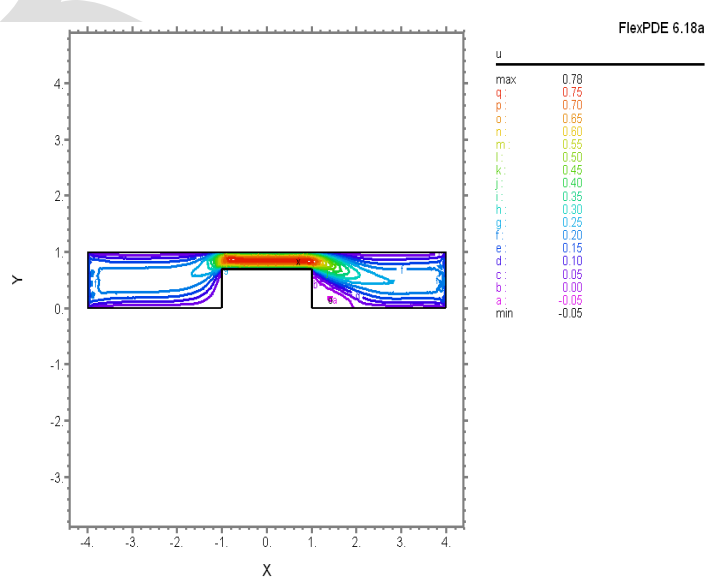
lowvisc: Grid#2 P2 Nodes=814 Cells=357 RMS Err= 1.0487
 Integral= 6.361090

Fig.12:Pressure at $h = 0.7$



lowvisc: Grid#2 P2 Nodes=813 Cells=358 RMS Err= 0.4566
 Integral= 0.474278

Fig.13:Streamlines at $h = 0.9$



lowvisc: Grid#2 P2 Nodes=813 Cells=358 RMS Err= 0.4566
 Integral= 1.270331

Fig.14:Velocity in x – direction at $h = 0.9$

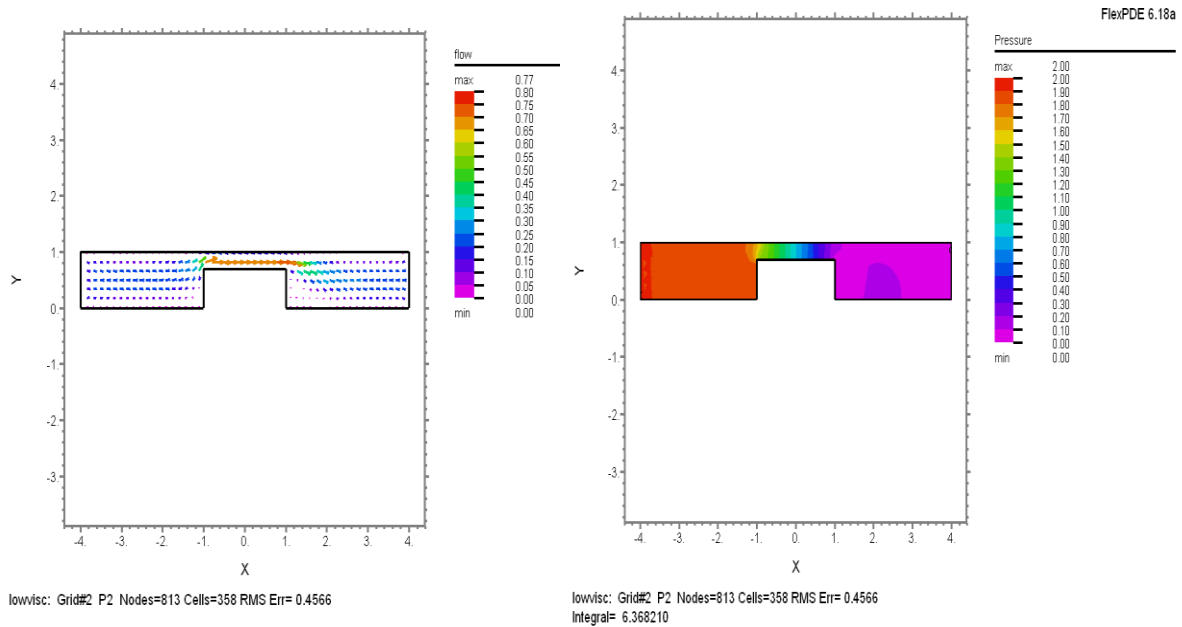


Fig.15:Flow at $h = 0.9$

Fig.16:Pressure at $h = 0.9$

CONCLUSION

The Flex PDE software was used for numerical simulation of fluid dynamics to evaluate the flow characteristics of incompressible viscous fluid i.e. water flowing in rectangular channel as laminar flow and obstructed by a solid rectangular obstruction (flat plate) of variable length using the Navier-Stokes equations alongwith continuity equation as an incompressibility constraint and the vorticity-stream function approach. In this study, it was found that there is a variation in the magnitude of the stream function due to different blockage ratios i.e. the maximum values of the stream function decreased with the increased in the blockage ratio and vice-versa. It was also observed that as we go away from the obstruction in the direction normal to the direction of flow, the value of function increased and by increasing the blockage ratio, the area in which the flow reverses its direction was found to be increased. It was also observed that with the increase in blockage ratio the region of low pressure increased behind the obstruction.

REFERENCES

- [1] Roshko, A. "On the wake and drag of bluff bodies." *J. Aero.Sci.* 22(2): 124 -132.1955.
- [2] Greenspan, D. "Numerical studies of steady, viscous, incompressible flow in a channel with a step." *J.Engg.Math.* 3(1):21-28.1969.
- [3] Zdravkovich, M.M. "Conceptual overview of laminar and turbulent flows past smooth and rough circular cylinders." *J. Wind Engg. and Industrial Aerodynamics*, 33: 53-62.1990.
- [4] Valencia, A. "Laminar Flow Past Square Bars Arranged Side By Side In A Plane Channel." Departamento de Ingeniería Mecánica Universidad de Chile Casilla 2777 Santiago, Chile
- [5] Braza, M., Chassaing, P. and Haminh, H. "Numerical study and physical analysis of the pressure and velocity fields in the near wake of a circular cylinder." *J. Fluid Mech.* 166: 79-130.1986.
- [6] Gera, B., Sharma, P.K. and Singh, R.K. "CFD analysis of 2D unsteady flow around a square cylinder" *Intern. J. Appl. Engg. Res.* 1(3):602-612. 2010.
- [7] Kumar, S., Cantu, C. and Gonzalez, B. "Flow past a rotating cylinder at low and high rotation rates." *J. Fluids Engg.* 133(4): doi.10.1115/1.4003984. 2011.
- [8] Lam, K.M. and Leung, M.Y.H. "Asymmetric vortex shedding flow past an inclined flat plate at high incidence." *Euro. J. Mech. B/Fluids* 24: 33-48.2005.
- [9] Vikram, C. K., Gowda, Y. T. and Ravindra, H.V. "Numerical simulation of two dimensional unsteady flow past two square Cylinders." *Intern. J. Tech. & Engg. Sys.* 2 (3):2011.
- [10] Doma, S.B., El-Sirafy, I.H. and El-Sharif, A.H. "Two-dimensional fluid flow past a rectangular plate with variable initial velocity." *Alexandria J. Math* 1(2): 36-57.2010.

- [11] Gowda, B.H.L. and Tulapurkaraz, E. G. "Reverse flow in a channel with an obstruction at the entry." J. Fluid Mech. 204: 229-244.1989.
- [12] Bhattacharyya,S.andMaiti,D. K. "Vortex shedding suppression for laminar flow past a square cylinder near a plane wall: a Two-dimensional analysis." ActaMechanica, 184: 15-31.2006.
- [13] Kabir, M.A., Khan, M.M.K. and Rasul, M.G. "Numerical modeling of reverse flow phenomena in a channel with obstruction geometry at the entry." WSEAS Trans.Fluid Mech. 3(3): 250 – 260.2008

IJERGS